Original Article

Regulation of Oxidative Stress Associated with an *SSK2* Point Mutation Promotes Amphotericin B Resistance in *Cryptococcus gattii*

Hengyu Deng[1,&], Xuefeng Zang[2,&], Enqi Zhao[2,&], Yemei Huang[3], Jing Liu[4], Yangyu Zhou[2], Chen Yang[5], Wencong He[6], Xiaozhuo Dong[4], Hui Chen[7], Ziqi Zhao[2], Yuhan Zhou[2], Xuelei Zang[4,#], Chen Wang[8,#], Liye Zhang[9,10,#], and Xinying Xue[2,4,#]

1. School of Medical Imaging, Shandong Second Medical University, Weifang 261053, Shandong, China; 2. Department of Respiratory and Critical Care, Xuanwu Hospital of Capital Medical University, National Clinical Research Center for Geriatric Diseases, Beijing 100053 China; 3. Department of Respiratory and Critical Care, Emergency and Critical Care Medical Center, Beijing Shijitan Hospital, Capital Medical University, Beijing 100038, China; 4. School of Clinical Medicine, Shandong Second Medical University, Weifang 261053, Shandong, China; 5. National Engineering Research Center of Immunological Products, Department of Microbiology and Biochemical Pharmacy, College of Pharmacy, Army Medical University, Chongqing 400038, China; 6. School of Information Science and Technology, ShanghaiTech University, Shanghai 201210, China; 7. School of Basic Medical Sciences, Shandong Second Medical University, Weifang 261053, Shandong, China; 8. Shanghai Key Laboratory of Molecular Imaging, Pudong Gongli Hospital, Shanghai University of Medicine and Health Sciences, Shanghai 201318, China; 9. School of Life Science and Technology, ShanghaiTech University, Shanghai 200032; 10. Shanghai Clinical Research and Trial Center, Shanghai 201210, China

Abstract

Objective *Cryptococcus gattii* (*C. gattii*) is a pathogenic respiratory fungus that rapidly disseminates through the central nervous system. The current clinical treatments for *C. gattii* infections are limited by prolonged therapeutic courses, high drug dosages, and insufficient antifungal options. This study aimed to explore the molecular mechanisms underlying amphotericin B (AmB) resistance in *C. gattii* and provide novel insights for developing targeted antifungal strategies.

Methods A total of 27 clinical *C. gattii* isolates were subjected to antifungal susceptibility testing, multilocus sequence typing (MLST) for phylogenetic analysis and resistance-related mutation screening. The CRISPR/Cas9 system was used to construct an *SSK2*-knockout mutant (*ssk2Δ*-G4). Capsule and melanin assays, murine pulmonary infection models, and transcriptomic analyses were performed to verify gene function, evaluate therapeutic efficacy, and explore the underlying regulatory mechanisms.

Results G4 isolates exhibited prominent AmB resistance with a novel *SSK2* c.793A>G missense mutation (p.Thr265Ala; hereafter *SSK2*^{T265A}). *SSK2* knockout significantly enhanced AmB susceptibility, whereas *SSK2*^{T265A} complementation partially restored the resistant phenotype. AmB treatment markedly reduced pulmonary fungal burden and inflammatory infiltration ($P < 0.05$) and improved survival ($P < 0.001$) in *ssk2Δ*-G4-infected mice. Mechanistically, this mutation upregulated *CAT1* expression and enhanced the reactive oxygen species–scavenging capacity and oxidative stress tolerance.

[&]These authors contributed equally to this work.

[#]Correspondence should be addressed to Xuelei Zang, E-mail: zangxuelei84@126.com; Chen Wang, E-mail: superlittlepig@sina.com; Liye Zhang, E-mail: zhangly@shanghaitech.edu.cn; Xinying Xue, PhD, Tel: 86-15210903118, E-mail: xuexinying@xwhosp.org

Biographical notes of the first authors: Hengyu Deng, M.Sc. majoring in pulmonary cryptococcal infection, drug resistance mechanisms, E-mail: 18790569782@163.com; Xuefeng Zang, PhD, majoring in respiratory infectious diseases, pulmonary cryptococcal infection, E-mail: zangxuefeng@xwhosp.org; Enqi Zhao, M.Sc. majoring in pulmonary cryptococcal infection, drug resistance mechanisms, E-mail: zeq4269@163.com

Conclusion *SSK2* c.793A>G is closely associated with AmB resistance and functionally contributes to the resistance phenotype. *SSK2* could serve as a potential therapeutic target for developing AmB synergistic sensitizers and as a research direction for future synergistic treatments of clinically resistant *C. gattii* strains.

Key words: *Cryptococcus gattii*; Amphotericin B; Drug resistance; *SSK2*; Oxidative stress; *CAT1*

Biomed Environ Sci, 2026; 39(10): 1200-1214 doi: 10.3967/bes2026.108 ISSN: 0895-3988

www.besjournal.com (full text) CN: 11-2816/Q *Copyright ©2026 by China CDC*

INTRODUCTION

Cryptococcus gattii (*C.gattii*) is a common opportunistic fungal pathogen that disseminates *via* the respiratory tract and causes pulmonary cryptococcosis. This pathogen spreads hematogenously to the central nervous system, leading to cryptococcal meningitis. In contrast to Cryptococcus neoformans (*C. neoformans*), which primarily infects immunocompromised hosts, *C. gattii* can also infect immunocompetent individuals, posing a distinct clinical challenge[1]. Currently, drugs used for the clinical treatment of fungal infections are primarily categorized into three classes. Among these, amphotericin B (AmB) is the only agent with direct fungicidal activity against *Cryptococcus* spp. It exerts its effect by binding to ergosterol in the fungal cell membrane, inducing a significant increase in intracellular reactive oxygen species (ROS) levels, and causing mitochondrial damage. Consequently, AmB plays a pivotal role in the treatment of refractory *Cryptococcus* infections[2]. Currently, precise clinical breakpoints for antifungal drugs targeting *Cryptococcus* spp. are lacking. To address this, Ordaya et al. analyzed temporal trends in minimum inhibitory concentrations (MICs) and proportions of wild-type (WT) isolates of *C. neoformans* complex processed by their reference laboratory between November 2011 and June 2021. They observed a higher mortality rate in patients infected with an AmB non-WT CNSC isolate[3]. Therefore, the clinical management of systemic cryptococcosis remains challenging.

The widespread use of antifungal drugs has led to the growing problem of fungal drug resistance[4]. Currently, the clinical application of antifungal agents is limited and therapeutic options for cryptococcal infections are particularly scarce. Therefore, screening and development of novel therapeutic targets are of great significance. Lee et al. performed systematic functional profiling of the kinome networks in *C. neoformans* by constructing a high-quality library of 264 signature-tagged gene-deletion strains *via* homologous recombination of 129 putative kinases and examining their phenotypic traits *in vitro* and *in vivo*. Their study provided insights into the pathobiological signaling circuitry of *C. neoformans* and identified potential anticryptococcal or antifungal drug targets. The mitogen-activated protein kinase (MAPK) pathway plays a key role in regulating fungal growth, stress response, apoptosis, and differentiation. Among these, the *SSK2* gene in *C. neoformans* serves as a crucial interface that links the two-component system to the PBS2-HOG1-MAPK pathway[5]. Targeted inhibition of *SSK2* can markedly enhance the fungicidal activity of AmB, reduce drug dosage and toxicity, and broaden its antifungal spectrum. It is a promising therapeutic target for addressing clinical AmB resistance and its adverse toxic effects.

This study comprehensively analyzed the relationship between drug-susceptibility phenotypes and phylogenetic relationships in 27 clinical *C. gattii* strains. Combined with *in vitro* and *in vivo* experiments, we revealed the molecular mechanism by which the $SSK2^{T265A}$ point mutation regulates AmB resistance in the G4 strains. This discovery not only elucidates a key evolutionary pathway for the emergence of clinical resistance in *C. gattii* but also provides crucial theoretical foundations and potential targets for developing novel antifungal drugs and synergistic treatment strategies against such resistant strains.

MATERIALS AND METHODS

Sources of Clinical Strain Samples

This study included 27 clinical isolates of *C. gattii*, all isolated from different patients and provided by multiple hospitals. The primary sample type was cerebrospinal fluid, with the remainder derived from the bronchoalveolar lavage fluid, sputum, blood, and lung tissues.

Bioinformatics Analysis

Strain Typing and Phylogenetic Analysis Raw whole-genome sequencing data for each strain were converted to FASTQ format using fastq-dump (v2.8.2, Bethesda, MD, USA), and quality control was performed using fastp (v0.20.0) to remove adapter sequences and low-quality reads. The filtered reads were aligned to the *C. gattii* WM276 reference genome (GenBank accession: GCF_000185945.1) using the Burrows-Wheeler Aligner BWA-MEM (v0.7.17). The resulting SAM files were sorted, converted to the BAM format using SAMtools, and then indexed. PCR duplicates were marked and removed using the MarkDuplicates tool in GATK (v4.3.0.0). Variant calling was subsequently performed for each sample using the HaplotypeCaller tool in GATK to generate the initial VCF files. Single-nucleotide polymorphisms (SNPs) were selected using the SelectVariants tool in GATK and filtered through the VariantFiltration tool using the following criteria: QUAL < 30.0 || QD < 2.0 || SOR > 3.0 || MQ < 40.0 || FS > 60.0. This process yielded high-confidence variant calls. Filtered VCF files from all samples were merged and converted to a PHYLIP format sequence alignment matrix using vcf2phylip, which was subsequently converted to the MEGA format using MEGA software (v11). A phylogenetic tree was constructed using the maximum parsimony method and strain molecular types were determined using the CHiPlot online tool.

Variant Calling, Filtering, and Annotation Raw sequencing reads were aligned to the *C. gattii* VGI reference genome WM276 (GenBank accession: GCF_000185945.1) using BWA-MEM (v0.7.17-r1188) and subsequently converted to the BAM format using SAMtools (v1.6). Initial variant calling was performed using the HaplotypeCaller tool in GATK (v4.2.6.1) to generate VCF files. SNP sites were extracted using the SelectVariants tool in GATK, followed by filtration with the VariantFiltration tool using thresholds (AB < 0.2 || MQ0 > 50) to remove low-quality variants. For subsequent analysis, variant sites were merged across samples using the GATK CombineGVCF tool. Variant sites were annotated and functionally characterized using SnpEff (v5.2) to predict gene effects and functional impacts in the G4 strain, which displays a pronounced resistance phenotype.

To identify candidate variants associated with AmB tolerance, whole-genome variants from strains G4 and G24 were subjected to stepwise filtering and prioritization rather than formal association testing. Variants were retained if they (i) occurred within coding regions, (ii) were predicted by SnpEff to have moderate or high functional impact[6], and (iii) involved genes previously implicated in virulence or antifungal resistance pathways[7,8]. Candidate variants were compared with the remaining clinical isolates to identify strain-specific enrichment patterns.

Molecular Genetics Experiments

Primer Design Accurate gene sequences were obtained from the NCBI database. The sequences were imported into Primer Express 3.0 for primer design, guaranteeing the primer length at 18–30 bp, GC content at 40%–60%, and Tm values of the forward and reverse primers ideally differing by no more than 2–5 °C. Finally, Primer-BLAST was used to align the primer sequences against corresponding genomic databases to confirm their uniqueness. The primer sequences used in this study are listed in Table 1.

CRISPR-Cas9-Mediated Gene Knockout To validate the functions of *SSK2* and *TCO2*, we constructed gene-knockout mutant strains using the G4 strain as the background. The target gene was knocked out using the CRISPR-Cas9-based TRACE system developed by Lin et al.[9]. Single-guide RNAs (sgRNAs) were designed to target the *SSK2* genomic locus. A donor DNA fragment containing homology arms and a nourseothricin (NAT) resistance marker was amplified by PCR. The CRISPR-Cas9 construct (containing the sgRNA expression cassette) and donor DNA fragment were co-introduced into *C. gattii* competent cells *via* electroporation. The transformed yeast culture was plated onto YPD agar containing 100 μg/mL NAT to select for NAT-resistant transformants. Genomic DNA was extracted from the putative positive clones and initially verified using NotI restriction digestion. PCR amplification and Sanger sequencing were performed to confirm the targeted gene deletion and precise integration of the homologous recombination cassette. The correct transformants were screened and used for subsequent functional studies.

Gene Complementation The *SSK2* complementation gene was cloned into a shuttle vector with a P_{H3} promoter using standard molecular cloning techniques to generate a recombinant plasmid. The recombinant plasmid was transformed into competent *Escherichia coli* cells *via* heat shock and plated onto LB agar plates containing the relevant antibiotic for the selection of positive clones. Single colonies were selected, and successful

insertion of the fragment was verified by colony PCR, followed by Sanger sequencing. The verified plasmid was linearized with an appropriate restriction enzyme and introduced into the *ssk2Δ*-G4 mutant strain *via* electroporation. Transformants were selected on YPD agar plates containing corresponding antibiotics to identify potential complementation strains. Successful genomic integration of *SSK2* was confirmed by diagnostic PCR and sequencing. The *SSK2* allele carrying the G4-derived *SSK2*^{T265A} point mutation was backcrossed into the knockout strain to generate *ssk2Δ*-G4+*SSK2*^{T265A}. A strain harboring the WT *SSK2* allele was obtained as *ssk2Δ*-G4+*SSK2*^{WT}, enabling the specific contribution of this point mutation to AmB resistance to be determined.

Phenotypic Analysis In Vitro

We determined the drug susceptibility of the strain, its ability to produce core virulence factors (capsule and melanin), and its tolerance to oxidative and osmotic pressure stress.

Antifungal Susceptibility Testing An initial phenotypic verification of the strains was conducted using the spot-test method. Subsequently, the MICs of the strains were determined using clinically standard fungal susceptibility test strips (E-test method) and the dilution method, as described by the Clinical and Laboratory Standards Institute (CLSI). All samples included three biological replicates and the experimental procedure was independently repeated three times.

Table 1. Primer sequences for gene deletion and gene complementation

Comments	Application name	Sequence
SSK2 deletion	Test-F	TGTGTCTTTGCTTGAACAATCGCTG
	Test-R	CCATAAGAGGTTTGAGAGGTTTTGA
	Left-se	CAGGTGGTGCTCTTGTG
	Left-an	CTGGCCGTCGTTTTACTATTCCCGTTCTTCTCC
	Right-se	GTCATAGCTGTTTCCTGAGATGTGCTCAGGGACT
	Right-an	AACAACGCTGCATGTTT
	U6-R	TCTTTGTGCGGTGTGCTTTCAACAGTATACCCTGCCGGTG
	gRNA-F	GAAAGCACACCGCACAAAGAGTTTTAGAGCTAGAAATAGCAAGTT
TCO2 deletion	Test-L	GGTTGAGTGAATGAGTTTATGG
	Test-R	TCAAACTTACTTCGTAATTCTGGTG
	Left-se	TGCGTCACAGACATCTATCG
	Left-anse	CTGGCCGTCGTTTTACTGGAAAGGCTCTGTTTATTG
	Right-se	GTCATAGCTGTTTCCTGTACACAGATGGGCGAAGGTT
	Right-anse	GACCAGGACGCCGCAGAGTTG
	g-RNA-F	ACCGCCTGGGATAGTAAGTTGTTTTAGAGCTAGAAATAGCAAGTT
	U6-R	AACTTACTATCCCAGGCGGTAACAGTATACCCTGCCGGTG
Universal primer	NAT1	CCGTCTTCACCTGCATCTGATT
	NAT2	TTGGATGCTGGATGCTGGGT
	U6 promoter -F	CCATCGATTTGCATTAGAACTAAAAACAAAGCA
	gRNA-R	CCGCTCGAGTAAAACAAAAAAGCACCGAC
	Cas9-F	GGTGACGCTGTGAGAGTGG
	Cas-R	GGGCCCCTCTTCACGTGG
SSK2 complementation	PH3-*ssk2*-Fse1	AGTACATTTATCACAGGCCGGCCATGTCCAATCCGACGTCCCC
	PH3-*ssk2*-Pac1	CTGCTACTGTAACCCTTAATTAATTATTCGAGGGGAGGTGTAATACC
	PH3-F	CCGTAATGCCTATTCTCCGAG

Note. F, forward; R, reverse; L, left; R, right; se, sequence; an/anse, anti/antisequence; Fse1, restriction endonuclease FseI; Pac1, restriction endonuclease PacI.

Spotting Test Experimental strains were inoculated into YPD liquid medium and incubated at 30 °C with shaking at 220 rpm for 16–18 h. Log-phase cultures were harvested, washed three times with sterile distilled water, resuspended in sterile physiological saline, and adjusted to a concentration of 5×10^7 CFU/mL (OD_{600} = 0.5). The cell suspension was subjected to serial five-fold dilutions of 5×10^7, 1×10^7, 2×10^6, 4×10^5, 8×10^4, and 1.6×10^4 CFU/mL, and 3-μL aliquots from each dilution were spotted onto YPD agar plates containing varying concentrations of antifungal agents (fluconazole, AmB, or 5-fluorocytosine). All plates were incubated at 30 °C for 48–72 h, with colony growth observed and recorded at regular intervals. Photographs were taken to document the growth phenotypes. Scores ranged from 0 (highly susceptible) to 2 (susceptible), 4 (increased resistance), and 6 (significantly increased resistance). This scoring system was used to quantify resistance based on the number of colonies grown in the drop plate assay.

E-Test Log-phase cultures (OD_{600} = 0.18 ± 0.02) were evenly inoculated onto RPMI 1640 agar plates using a sterile cotton swab with a three-way cross-streaking technique. After allowing the agar surface to dry briefly, an E-test strip (AmB concentration range: 0.002–32 μg/mL) was aseptically placed horizontally onto the agar using sterile forceps[10]. The plates were incubated at 35 °C for 72 h, after which the MIC was recorded.

MIC-CLSI C. gattii was inoculated into YPD medium and cultured at 30 °C for 15 h. Fungal cells were collected by centrifugation and washing, then diluted to 2.5×10^3 CFU/mL in RPMI 1640 medium (0.145 mol/L MOPS buffer). Serial two-fold dilutions of the antifungal compounds were prepared in RPMI 1640 medium in a 96-well plate and then mixed with equal volumes of the prepared fungal cell suspension. The 96-well plates were incubated at 30 °C for 48 h. Wells containing only RPMI as a blank were prepared, along with wells containing fungal cell-RPMI mixture as a control within the same plate.

Assessment of Capsule Formation Capacity A 30-μL aliquot of log-phase culture (4×10^7 CFU/mL) was inoculated into 1 mL of complete DMEM medium and incubated statically at 37 °C under 5% CO_2 for 72 h to induce capsule formation. Following incubation, 10 μL of culture was mixed with an equal volume of India ink for slide preparation. The slides were observed and imaged under a light microscope with 100× oil immersion[11].

Assessment of Melanin Production Capacity A 3-μL aliquot of log-phase culture (OD_{600} = 2.0 ± 0.1) was inoculated onto melanin-inducing agar plates containing 1 mmol/L L-DOPA and the following components: 15 mmol/L glucose, 13 mmol/L glycine, 29.4 mmol/L KH_2PO_4, 10 mmol/L $MgSO_4 \cdot 7H_2O$, and 3 mmol/L thiamine. The plates were incubated in the dark at 30 °C for 48 h after the inoculum was completely absorbed. Colony pigmentation was observed daily, and phenotypic characteristics were recorded[12].

Hydrogen Peroxide Killing Assay The test strain was inoculated into YPD liquid medium and incubated at 30 °C with shaking at 220 rpm for 14 h until the logarithmic growth phase was reached. The concentration of the suspension was adjusted to an OD_{600} of 0.4. A solution containing 0.015% H_2O_2 was then added and incubated for 2 h. Then, 1 mL of the suspension was serially diluted, and the dilutions were spread onto YPD plates. After 48 h of incubation, CFU counts were recorded and photographs were used to document strain survival. This experiment included three biological replicates, each performed in triplicate.

Phenotypic Analysis In Vivo

Animal Infection Model and Therapeutic Efficacy Evaluation Eighty 8-week-old female C57BL/6N mice (SPF) were randomly assigned to four groups (n = 20 per group) using a random number table. Following anesthesia by intraperitoneal injection of tribromoethanol (250 mg/kg), mice were intranasally inoculated with 40 μL of a *C. gattii* suspension (1×10^7 CFU). Beginning on day 1 post-infection (dpi), the mice in the treatment group received daily intraperitoneal injections of AmB [3 mg/(kg·d)]. In contrast, control mice received an equal volume of phosphate-buffered saline (PBS) for 7 consecutive days. The experimental endpoints were as follows: 5 mice per group were euthanized post-treatment for the collection of lung and brain tissues to quantify the fungal burden. Six mice per group were euthanized on days 7 (early stage) and 30 (late stage) for histopathological analyses. The survival of the remaining 9 mice per group was monitored.

Quantification of Fungal Burden in Lung Tissue Under sterile conditions, lung tissues were dissected and transferred to a sterile tissue homogenizer containing 3 mL ice-cold PBS and 3-mm grinding beads. Homogenization was performed for 2 min. The homogenate was serially diluted 10-fold (10^{-1} to 10^{-3}) in PBS. A 100-μL aliquot from each dilution was spread plated onto YPD agar plates supplemented with chloramphenicol (50 μg/mL). The plates were incubated at 30 °C for 72 h, and the CFUs were

enumerated.

Histopathological Analysis On days 7 and 30 post-infection, lung tissues were collected from euthanized mice in each group and fixed for paraffin embedding. Tissue sections (4–5 μm thickness) were prepared and stained using the following protocols for histopathological analysis: hematoxylin and eosin (H&E) staining, periodic acid–Schiff (PAS) staining, and Alcian blue (AB) staining.

Survival Analysis Mice were group-housed in separate cages (5 mice per cage) in an ABSL-2 facility. Health monitoring was performed twice daily to assess activity level, fur condition, respiratory status, and food and water consumption. The experiment was continued for 80 days or until humane endpoints were met (e.g., > 20% body weight loss, severe respiratory distress, or immobility). Kaplan–Meier survival curves were generated, and between-group differences in survival rates were analyzed using the log-rank test.

LC-MS/MS-Based Ergosterol Quantification The biomass from each strain was collected, vacuum-dried, and mechanically disrupted using a tissue homogenizer with ceramic beads (5 cycles of 40 s each). To the homogenized sample, 1 mL of chloroform containing ketoconazole (2.5 μg/mL) as an internal standard was added. The mixture was then incubated at room temperature with shaking for 8 h. After extraction, the solvent was concentrated under vacuum, dried, and reconstituted in methanol/chloroform (10:1, v/v). The solution was vortexed and centrifuged at 12,000 ×*g* for 5 min. The supernatants were collected for subsequent analysis. The high-performance liquid chromatography (HPLC) conditions were as follows: mobile phase A, 0.01% acetic acid; mobile phase B, acetonitrile; chromatographic column, C18 (2.1 mm × 50 mm, 1.8 μm); flow rate, 0.4 mL/min; column temperature, 45 °C. The elution program was as follows. Initially, 30% A + 70% B was used. After 1 min, the phase was switched to 100% B for 16 min. At 17 min, the phase was switched back to 30% A + 70% B and the column was equilibrated for 6 min. Mass spectrometry was performed using an Agilent 6520B analyzer (Agilent Technologies, Santa Clara, CA) in Q-TOF MS Ionization mode, APCI positive ion mode, drying gas flow rate of 4 L/min, nebulizer temperature of 350 °C, nebulizer pressure of 50 psi, capillary voltage of 3,500 V, fragmentation voltage of 130 V, scan range of 80–1,000 m/z, and acquisition frequency of 1.03 spectra/s. Ergosterol assays were performed with three independent biological replicates, and each sample was analyzed in triplicate.

Analysis of AmB-Induced ROS Levels Tested strains were inoculated into YPD liquid medium and incubated at 30 °C with shaking at 220 rpm for approximately 14 h to reach the logarithmic growth phase. The cells were harvested by centrifugation, washed with fresh YPD medium, and resuspended. The cell suspension was adjusted to a standardized concentration (OD_{600} = 0.5) and treated with various AmB concentrations. The cultures were incubated with shaking (30 °C, 220 rpm) for 1 h. After treatment, cells were collected, washed twice with PBS, and resuspended in 10 μg/mL DCFH-DA, then incubated at 37 °C in the dark for 1 h. Fluorescence intensity was measured by flow cytometry for each experimental group. The excitation wavelength was 488 nm and emission was detected at 510–560 nm. ROS assays were performed with three independent biological replicates, and each sample was analyzed in triplicate.

RNA Extraction and Transcriptome Sequencing Analysis RNA-seq was performed on three independent biological replicates per group. The strains (G4 and the *ssk2Δ*-G4 mutant) were separately inoculated into YPD liquid medium and incubated at 30 °C with shaking at 220 rpm for 14–16 h to reach the mid-logarithmic growth phase (OD_{600} = 0.8). After incubation, 3 mL of culture from each strain was collected and centrifuged, and the cell pellet was washed twice with sterile PBS. The following treatment groups were prepared: Control group: Resuspended in 4 mL of fresh YPD medium (designated G4-YPD and *ssk2Δ*-G4-YPD); Treatment group: Resuspended in 4 mL of YPD medium containing 0.5 μg/mL AmB (designated G4-AmB and *ssk2Δ*-G4-AmB). All groups were incubated at 30 °C for 3 h with shaking at 220 rpm. After treatment, the cells were harvested, washed with nuclease-free water, and flash-frozen in liquid nitrogen. Frozen pellets were stored at −80 °C until RNA extraction and subsequent transcriptomic sequencing.

Quality control was performed using an Agilent 2100 Bioanalyzer to precisely assess RNA integrity. Leveraging the structural characteristics of the poly(A) tail, mRNA containing poly(A) tails was enriched with oligo(dT) magnetic beads. Following enrichment, library preparation was performed using either the standard NEB method or the strand-specific method[13]. After library construction, preliminary quantification was performed using a Qubit 2.0 fluorometer (Thermo Fisher Scientific, Waltham, MA). The library was diluted to 1.5 ng/μL, and the insert sizes were assessed using an Agilent

2100 Bioanalyzer. Once the insert size met the expectations, we accurately quantified the effective library concentration *via* qRT-PCR before proceeding with Illumina sequencing. qPCR data are presented as mean ± SD from three biological replicates (n = 3 per group), each performed in technical triplicates.

Statistical Analysis

All statistical analyses were performed using GraphPad Prism (version 9.0; GraphPad Software, San Diego, CA). A P value < 0.05 was considered statistically significant. Normality and homogeneity of the variance were tested. Independent-samples t-tests were used for comparisons between two groups of continuous variables that met normality assumptions, while one-way analysis of variance was employed for comparisons among multiple groups. Survival curves were plotted using the Kaplan–Meier method, and intergroup survival rate comparisons were performed using the log-rank test. All statistical analyses were considered significant at $P < 0.05$, with the results annotated in figures and tables using asterisks (* $P < 0.05$, ** $P < 0.01$, and *** $P < 0.001$).

RESULTS

The G4 Strain Harbors the Key Point Mutation SSK2^{T265A}

A total of 27 clinical *C. gattii* isolates derived from clinical samples were included in this study. Multilocus sequence typing analysis classified 20 isolates as VGI and 7 as VGII. Phylogenetic reconstruction indicated that strain G4 had the closest genetic relationship with strain G24 (Figure 1A). Antifungal susceptibility testing demonstrated that G4 exhibited increased resistance to AmB compared with other clinical isolates, including the phylogenetically closest strain, G24 (Figure 1B, Supplementary Figure S1, Supplementary Table S1).

To investigate the genetic basis of AmB tolerance in G4, whole-genome sequencing and comparative analyses were performed between G4 and the closely related AmB-susceptible strain, G24 (Figure 1B). In total, 2,223 unique SNPs were identified in G4. Subsequent comparative variant filtering and candidate prioritization analysis indicated that three SNPs correlated with AmB susceptibility, narrowing the candidate loci to two genes, *SSK2* and *TCO2*. Comparative sequence alignment across the remaining 25 clinical *C. gattii* isolates revealed that the *SSK2*^{T265A} variant was uniquely enriched in G4, whereas no lineage-specific enrichment was observed for *TCO2* variants (Figure 1C, Supplementary Figure S2, Supplementary Table S2).

SSK2^{T265A} Mutation Affects the Susceptibility of G4 Strain to AmB

Spot-on-plate assays showed that *ssk2Δ*-G4 exhibited pronounced growth inhibition on medium containing 0.5 μg/mL AmB compared with parental G4 (Figure 2A). Similarly, *SSK2* deletion in six VGIb clinical isolates produced comparable AmB-sensitive phenotypes (Figure 2B). These findings suggest that stress adaptation processes involving Ssk2 are broadly conserved across *C. gattii* strains.

Complementation of *ssk2Δ*-G4 with the mutant allele *SSK2*^{T265A} largely restored AmB tolerance to parental levels, whereas complementation with the WT allele *SSK2*^{WT} produced susceptibility similar to the reference sensitive strain WM276. E-test strip assays and the CLSI method corroborated these findings.

Specifically, the E-test strip assay demonstrated that G4 exhibited an MIC of 0.38 μg/mL. The MIC of the *ssk2Δ*-G4 mutant decreased to 0.125 μg/mL, whereas the *SSK2*^{T265A} strain restored the MIC comparable to that of the G4 strain. Additionally, the *SSK2*^{WT} strain displayed an MIC consistent with that of the reference strain WM276 (Figure 2C, D). The results of the CLSI method showed that the MIC for G4 was 1.56 μg/mL, decreased to 0.78 μg/mL in *ssk2Δ*-G4, and returned to 1.56 μg/mL upon complementation with *SSK2*^{T265A} (Figure 2E). These findings indicate that the point mutation in *SSK2* in strain G4, which causes the *SSK2*^{T265A} amino acid substitution, is closely associated with the AmB resistance phenotype.

Deletion of SSK2 Affects Stress Tolerance and Virulence in C. gattii

The *ssk2Δ*-G4 mutant exhibited significantly impaired growth compared with the G4 strain, indicating reduced nitrosative stress tolerance (Supplementary Figure S3A). The mutant strain also exhibited heightened sensitivity to high osmolarity and cell wall stress. It displayed markedly suppressed growth in media with elevated NaCl/KCl concentrations and pronounced growth defects on SDS- or Congo red-supplemented plates, suggesting compromised cell wall integrity (Supplementary Figure S3B). Furthermore, *SSK2* deletion significantly altered the virulence-associated phenotypes of *C. gattii*. Compared with the G4 strain, the *ssk2Δ*-G4 mutant exhibited an enlarged and diffuse capsular structure and increased

melanin production, indicating that *SSK2* contributes to the regulation of virulence-associated traits (Supplementary Figure S3C). Additionally, melanin production was significantly higher than in the G4 strain (Supplementary Figure S3D). Notably, *SSK2* deletion did not impair growth at 37 °C (Supplementary Figure S3E). These findings indicate that *SSK2* modulates AmB resistance in *C. gattii* and plays a crucial role in maintaining diverse stress-response capacities and virulence phenotypes.

SSK2 Deletion Enhances the In Vivo Efficacy of AmB Treatment

To evaluate the effect of Ssk2 protein function on the efficacy of AmB treatment in *C. gattii* infection, we established a mouse respiratory tract mucosal infection model to compare the outcomes of different fungal strains under AmB treatment (Figure 3A).

During the early phase of infection (day 7), the lung tissue of PBS-treated control mice exhibited generalized enlargement, with scattered dark red necrotic foci visible on the surface and localized punctate areas of hyalinization. In contrast, the lung tissue from AmB-treated mice appeared pink and soft, with no significant enlargement or necrotic lesions (Figure 3B). Histopathological damage was reduced (Figure 3C), with markedly decreased inflammatory cell infiltration and necrotic foci ($P < 0.05$) (Figure 3D).

By the late stage of infection (day 30), the lung tissue volume in control mice increased significantly, with the surface extensively covered by mucous

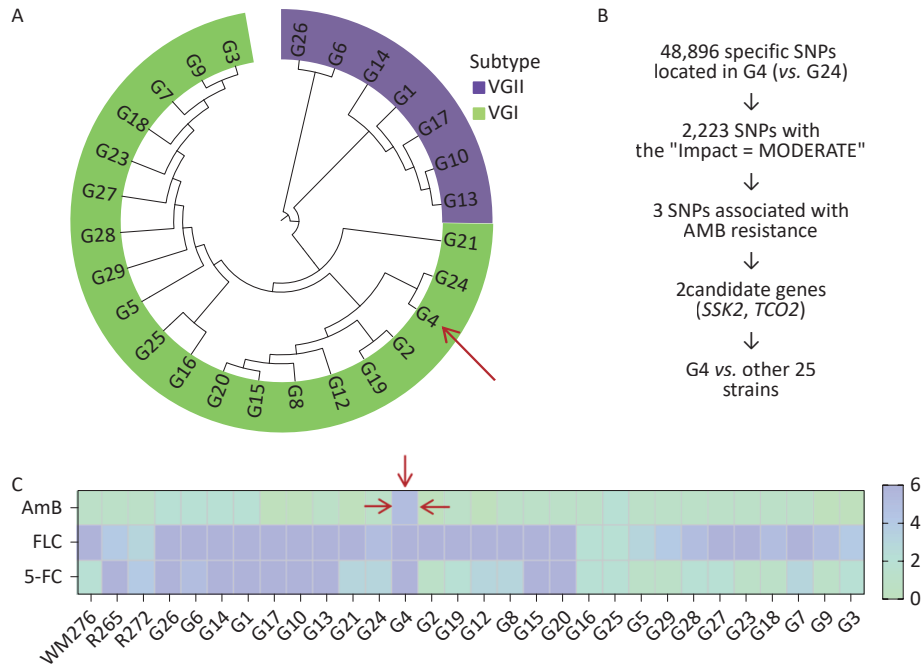


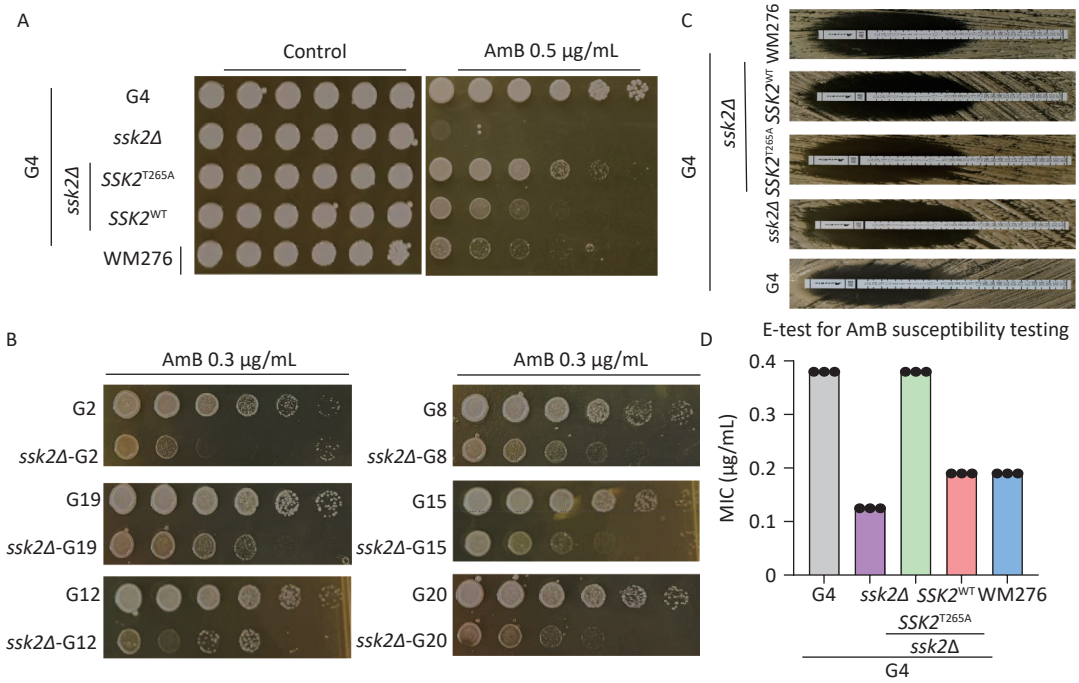
Figure 1. Integrated phenotypic and genomic analyses identify an *SSK2* point mutation associated with amphotericin B resistance in *Cryptococcus gattii* G4. (A) Phylogenetic tree analysis of 27 clinical *C. gattii* isolates. Green indicates VGI genotype; purple indicates VGII genotype. The arrow points to the AmB-resistant G4 strain. (B) Analysis of susceptibility to three clinical therapeutic agents—AmB, 5-fluorocytosine, and fluconazole—across various strains. Purple indicates increased resistance, green indicates susceptibility. Scores range from 0 (highly susceptible) to 2 (susceptible), 4 (increased resistance), and 6 (significantly increased resistance). The 0–6 scoring system quantifies resistance based on the number of colonies grown in the drop plate assay. Spot-on-plate results are shown in Supplementary Figure S1. The susceptibility results for drugs across strains correspond to the following fungal suspension concentrations: 5×10^7, 1×10^7, 2×10^6, 4×10^5, 8×10^4, and 1.6×10^4 CFU/mL. In the AmB results, after five successive five-fold serial dilutions, colonies of strain G4 could still grow. In contrast, other strains only survived at the original concentration and exhibited no colony growth at all the diluted concentrations. G4 exhibits significantly greater resistance to AmB than other strains. (C) Screening process for genes causing resistance variation in the G4 strain. AmB, amphotericin B; CFU, colony-forming units.

edema, appearing grayish-white and markedly hardened. Although the lung tissue volume of the treated mice did not change significantly, a certain degree of necrosis and consolidation was still observed in the lung lobes of mice infected with the G4 strain and treated with AmB. Notably, mice infected with the *SSK2*-deficient strain and treated with AmB maintained the soft lung tissue texture without observable pathological changes, including necrosis, hemorrhage, or consolidation (Figure 3E). Histopathological damage was reduced (Figure 3F), with markedly decreased inflammatory cell infiltration and necrotic foci ($P < 0.05$) (Figure 3G).

The results showed that after AmB treatment, the difference in fungal burden between mice infected with G4 and those infected with the *ssk2Δ*-G4 mutant strain was statistically significant in both groups. However, the reduction in pulmonary fungal burden was more pronounced in mice infected with the *ssk2Δ*-G4 mutant strain ($P < 0.05$) (Figure 3H, I). Survival rates were significantly improved in the treated mice ($P < 0.001$) (Figure 3J).

SSK2^{T265A} Enhances AmB Resistance through Reinforced ROS Homeostasis

Under hydrogen peroxide (H_2O_2)-induced oxidative stress, the *ssk2Δ*-G4 mutant strain exhibited a markedly reduced survival rate and a near-complete



E

Strain	MIC (μg/mL)	MFC (μg/mL)
G4	1.56	1.56
ssk2Δ-G4	0.78	0.78
ssk2Δ-G4 + *SSK2*^{T265A}	1.56	1.56
ssk2Δ-G4 + *SSK2*^{WT}	0.78	0.78
WM276	0.78	0.78

Figure 2. *In vitro* functional validation of *SSK2* CLSI, Clinical and Laboratory Standards Institute; YPD, yeast extract peptone dextrose medium; MIC, minimal inhibitory concentration. (A) Cells cultured overnight were spotted onto YPD medium. *SSK2*^{T265A} denotes the strain *ssk2Δ*-G4+*SSK2*^{T265A}; *SSK2*^{WT} denotes the strain *ssk2Δ*-G4+*SSK2*^{WT}. (B) *SSK2* knockout in six clinical strains of *C. gattii* VGI resulted in increased sensitivity to AmB. (C) MIC of AmB for each strain was measured using the E-test. (D) Quantitative analysis of the results presented in panel C. (E) Measurement of the AmB MIC against *C. gattii* using the CLSI method. Representative results from one of three independent experiments are shown. AmB, amphotericin B; CLSI, Clinical and Laboratory Standards Institute; MIC, minimum inhibitory concentration; WT, wild type; YPD, yeast extract peptone dextrose medium.

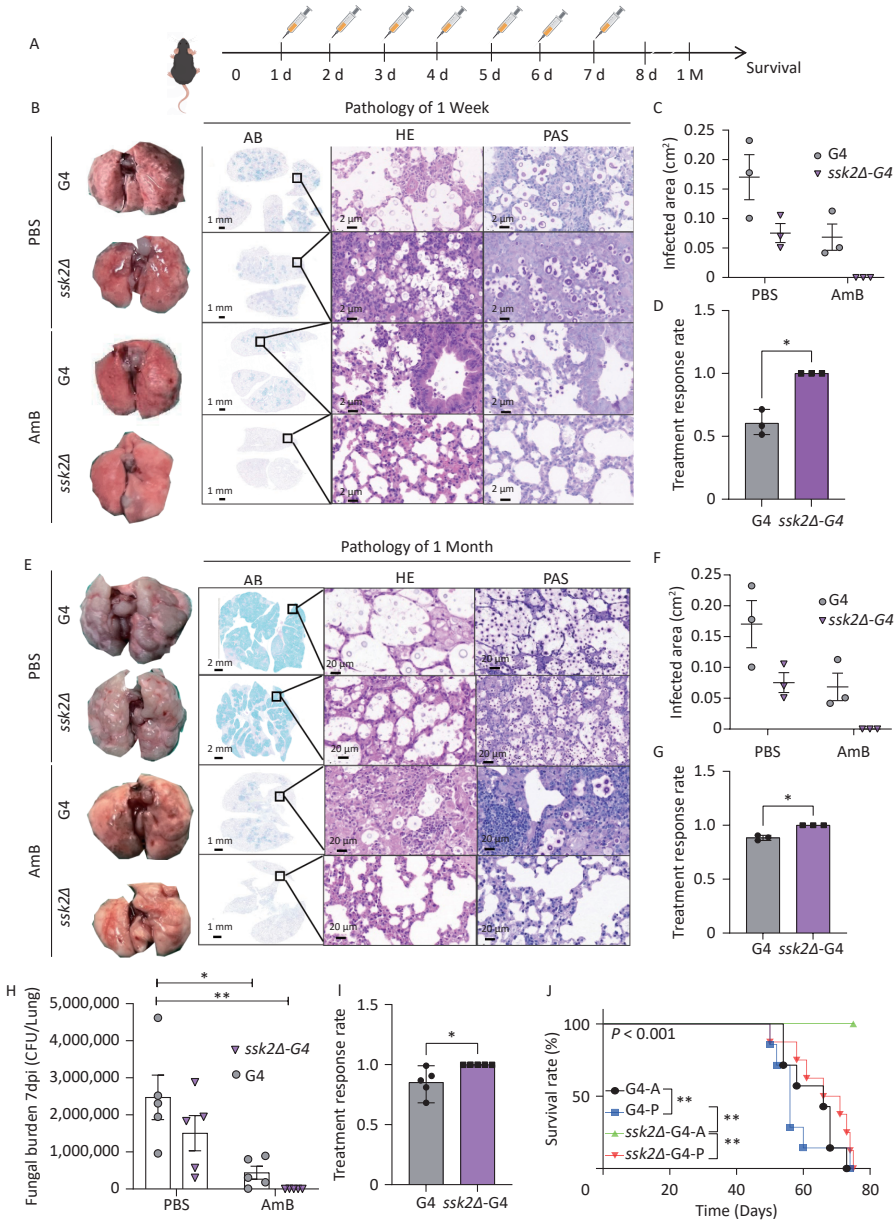


Figure 3. Functional validation of *SSK2 in vivo.* (A) Schematic of the experimental design. (B) Histopathological examination of the lungs using H&E, PAS, and AB staining one week post-modeling. Arrows indicate the sites of *Cryptococcus gattii* infection. (C) ImageJ measurement of the infected lung area in mice. (D) Compared to G4, *ssk2Δ*-G4 mice showed significantly greater reduction in lung infection area after drug treatment ($P < 0.05$). (E) Histopathological changes in the lung tissue one month after modeling. (F) ImageJ measurement of the infected lung area in mice. (G) At 1 month, *ssk2Δ*-G4 inhalation reduced lung infection area and improved efficacy *vs*. G4 ($P < 0.05$). (H) Fungal burden of the total lung homogenate after 7-day i.p. AmB [3 mg/(kg·d)]. The *ssk2Δ*-G4-AmB group showed lower burden ($P < 0.05$). (I) *ssk2Δ*-G4-infected mice exhibited greater fungal burden reduction and efficacy *vs*. G4 controls post-treatment ($P < 0.05$). (J) Survival curves were compared using the log-rank (Mantel–Cox) test ($P < 0.001$). The histopathological experiments were conducted using 3 mice per group. Fungal burden experiments were conducted with 5 mice per group. Survival experiments were conducted with 9 mice per group. Two-tailed paired Student's *t*-test was used for panels D, F, G, and I. AB, Alcian blue; AmB, amphotericin B; H&E, hematoxylin and eosin; i.p., intraperitoneal; PAS, periodic acid–Schiff; PBS, phosphate-buffered saline.

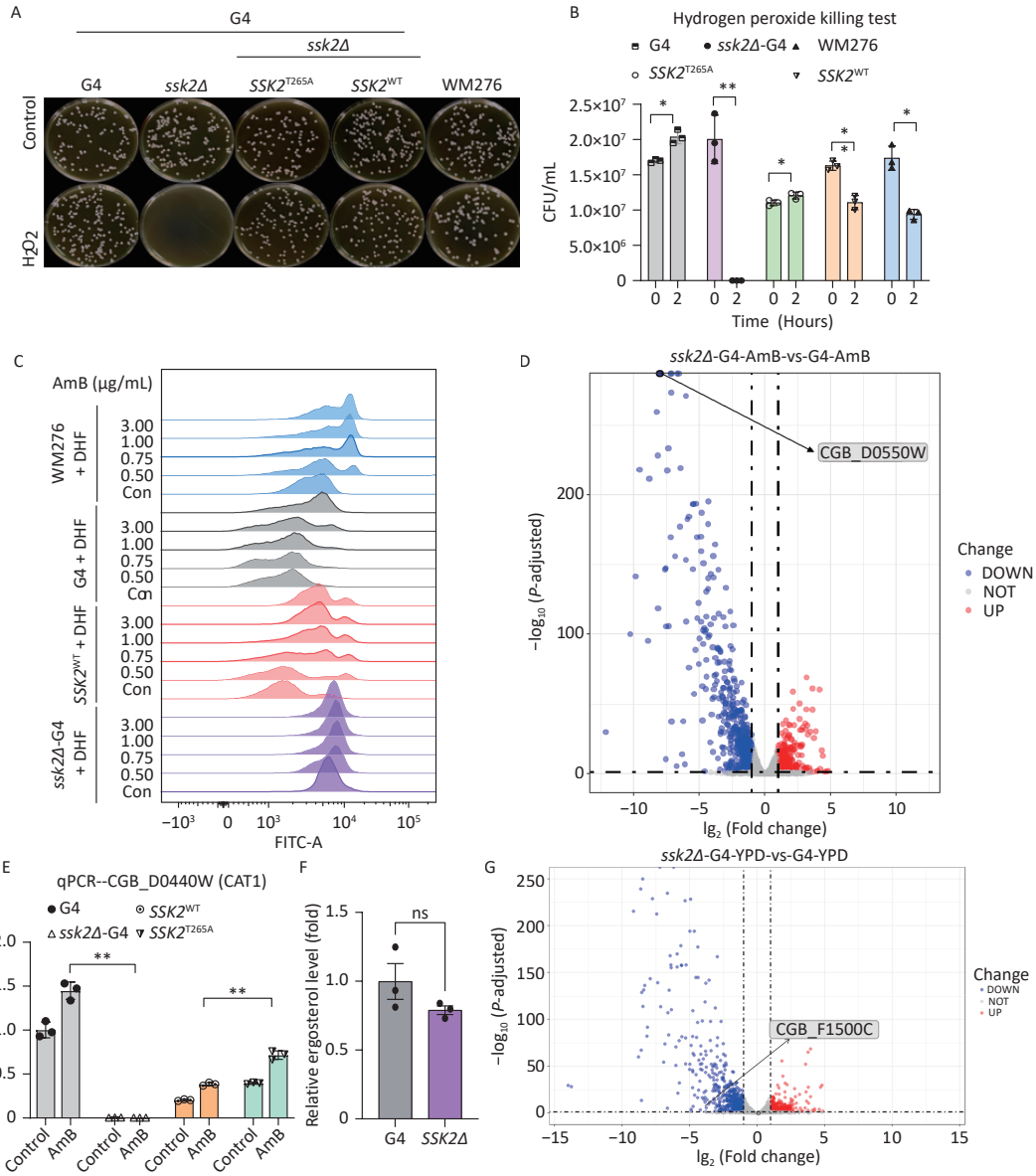


Figure 4. The role of *SSK2* in regulating the AmB sensitivity mechanism in *Cryptococcus gattii.* (A) Fungal colony growth results showing surviving colonies of each strain after 2 h of 0.015% H_2O_2 stress. (B) After 2 h of 0.015% H_2O_2 stress, *ssk2Δ*-G4 exhibited complete loss of activity. (C) DCFH-DA fluorescence assay analysis of ROS production levels in each strain under AmB-induced conditions. D: Under AmB stress, *ssk2Δ*-G4 markedly downregulated *CAT1* (log_2FC = −8.02 *vs*. G4, arrows). (E) qPCR validation of *CAT1* (CGB_D0440W) showed that *CAT1* was reduced in *ssk2Δ*-G4, while *ssk2Δ*-G4+*SSK2*^{T265A} exhibited higher *CAT1* levels than *ssk2Δ*-G4+*SSK2*^{WT}. The transcripts were normalized to actin and calibrated to G4 in YPD (set to 1.0). Data are mean ± SD (*n* = 3 biological replicates). (F) Under the current experimental conditions, after knocking out *SSK2*, the ergosterol content of the strain did not change significantly (*P* > 0.05). (G) Under YPD culture conditions, after deletion of *SSK2* in the G4 strain, the expression level of the ergosterol biosynthesis-related gene *ERG5* (CGB_F1500C) showed no significant change (*P* > 0.05). Two-tailed paired Student's *t*-test was used for panels B, E, and F. AmB, amphotericin B; DCFH-DA, 2′,7′-dichlorodihydrofluorescein diacetate; log_2FC, log_2 fold change; qPCR, quantitative polymerase chain reaction; ROS, reactive oxygen species; SD, standard deviation; YPD, yeast extract peptone dextrose medium.

loss of viability (Figure 4A). In contrast, the complemented strain *ssk2Δ*-G4+*SSK2*^{T265A} retained the ability to form colonies under identical conditions, indicating a restored growth capacity. Both the *ssk2Δ*-G4+*SSK2*^{WT} strain and the WM276 reference strain exhibited substantial growth inhibition, with a significantly reduced colony-forming capacity (Figure 4B). These results indicated that the *SSK2*^{T265A} mutation enhanced fungal tolerance to peroxide-induced oxidative stress.

Further flow cytometric analysis revealed that the G4 strain maintained relatively low basal levels of intracellular ROS following stimulation with AmB and other agents, with a significant increase in ROS accumulation observed only at a high drug concentration (3 μg/mL). In contrast, the *ssk2Δ*-G4 mutant exhibited markedly increased sensitivity to oxidative stress, demonstrating substantial ROS accumulation even at a sub-inhibitory concentration of 0.5 μg/mL (Figure 4C).

RNA-seq and qPCR analysis revealed that *SSK2* deletion downregulated the expression of genes encoding antioxidant enzymes. Compared to the G4 strain, the *ssk2Δ*-G4 mutant exhibited significant downregulation of 2,070 genes, including the key antioxidant gene *CAT1* (CGB_D0440W), which showed markedly reduced expression (log_2FC = −8.018, *Padj* < 0.001; Figure 4D). qPCR confirmed that *CAT1* transcription was significantly reduced following *SSK2* deletion (Figure 4E). It is worth noting that the quantitative analysis of ergosterol content in the strains showed that there was no significant difference in ergosterol content between the *ssk2Δ*-G4 mutant and G4 (*P* > 0.05) (Figure 4F). The transcriptomic data also indicated that after the deletion of *SSK2*, *ERG5* expression (CGB_F1500C), which is involved in ergosterol synthesis, did not show significant changes (Figure 4G). Our findings support a role for *SSK2* in the regulation of oxidative stress homeostasis and AmB susceptibility in *C. gattii*. The higher *CAT1* expression observed in the *ssk2Δ*-G4+*SSK2*^{T265A} strain compared with the *ssk2Δ*-G4+*SSK2*^{WT} strain further suggests that the *SSK2*^{T265A} allele contributes to enhanced oxidative stress regulation. However, additional allele-specific sterol profiling and downstream functional validation are required to determine whether the *SSK2*^{T265A} mutation directly regulates *CAT1* expression and to fully exclude sterol-associated contributions.

Effects of SSK2 Knockout on Transcriptional Expression of Downstream Genes

To elucidate the molecular network mechanism by which *SSK2* regulates AmB drug sensitivity in *C. gattii,* we performed RNA-seq analysis of the transcriptomes of G4 and the *ssk2Δ*-G4 mutants under AmB stress. Principal component analysis (PCA) revealed that the two sample groups were clearly distinguishable along the primary component PC1 (contributing 49.1% of the variance) (Supplementary Figure S4A). Differentially expressed genes were screened using the thresholds $|log_2FC| > 2$ and *Padj* < 0.05. Through Venn diagram intersection analysis, three key gene sets were defined: Set 1, containing 451 genes upregulated explicitly in the G4 strain under AmB stress; Set 2, containing 872 genes not upregulated in the *ssk2Δ*-G4 strain under AmB stress (compared to G4); and Set 3, containing 2,070 genes significantly downregulated in the *ssk2Δ*-G4 strain relative to G4 under AmB stress. Re-intersecting these three gene sets yielded 49 core differentially expressed genes (Supplementary Figure S4B). Gene Ontology functional enrichment analysis of these 49 genes revealed that *SSK2* deletion primarily disrupted processes related to DNA replication and metabolism, significantly impairing molecular functions such as drug and ATP binding (Supplementary Figure S4C, D). The raw sequencing data from this study are publicly available at the National Microbial Science Data Center (https://nmdc.cn/).

DISCUSSION

SSK2^{T265A} *is a Biologically Significant Marker of Drug Resistance Potential*

In the results of measuring the MICs of the strains, the absolute MIC differences between the E-test and CLSI methods may be attributable to methodological variations; nevertheless, both methods consistently show that G4 exhibits increased resistance relative to the *ssk2Δ*-G4 mutant, and the trends are in agreement. Generally, the CLSI method for determining MIC in the laboratory is the method of choice for monitoring resistance to antifungal drugs. The E-test and CLSI broth microdilution are not directly interchangeable; therefore, we based our primary interpretation on the CLSI reference method. However, owing to the lack of interpretive breakpoints, antifungal resistance in *Cryptococcus* spp. is difficult to define in the laboratory. Using the epidemiological cutoff values (ECVs) established through global multicenter studies as a benchmark, this study investigated the antifungal susceptibility patterns of *Cryptococcus* isolates and their association with epidemiological

characteristics[14,15]. This study found that strains carrying the *SSK2*^{T265A} mutation had MIC values measured using the CLSI method that were higher than the ECV threshold, suggesting that this mutation may have led to the strain acquiring low-level resistance. Although this absolute MIC shift may seem small, Bicanic et al. confirmed that *Cryptococcus* spp. undergo a small but significant drift in AmB MIC during clinical recurrence, which is associated with treatment failure[16]. Therefore, the slow increase in MIC driven by the point mutation revealed in this study represents the functional activation of an early resistance mechanism and has important evolutionary biological significance.

AmB Exhibits Therapeutic Efficacy Against G4 but Demonstrates Even more Pronounced Therapeutic Effects Against ssk2Δ-G4

In the PBS control group, mice infected with the *ssk2Δ*-G4 mutant strain exhibited higher lung fungal burden and more severe pulmonary infection than those infected with the G4 strain. *SSK2* gene is a key component of the MAPK signaling pathway and serves as the core interface between the two-component system and PBS2-HOG1 pathway. It simultaneously regulates fungal drug susceptibility and the synthesis of virulence factors such as capsules and melanin. Specifically, *SSK2* negatively regulates capsular biosynthesis and melanin production. Consequently, infection with the *ssk2Δ*-G4 mutant strain exacerbates pulmonary tissue damage in mice. However, *SSK2* deficiency significantly enhanced susceptibility to AmB in *C. gattii*. Following AmB treatment, while lung lesions in mice infected with the G4 strain were largely cleared, those infected with the *ssk2Δ*-G4 mutant exhibited near-complete eradication of *C. gattii* in lung tissue. Pathological sections showed no significant lesion formation, indicating markedly improved survival outcomes. In summary, although AmB exhibited fungicidal activity against the G4 strain, *SSK2* deletion further enhanced its *in vivo* efficacy.

SSK2^{T265A} *Functionally Contributes to the AmB Resistance Phenotype in C. gattii by Affecting CAT1 Expression*

Under the action of AmB, the ergosterol content in the *ssk2Δ*-G4 mutant strain showed no significant change. Ssk2 is a key upstream kinase of the HOG pathway and belongs to the MAPKKK family. *Cryptococcus* spp. receive upstream signals and activate downstream Pbs2 (MAPKK) and Hog1 (MAPK) through a phosphorylation cascade, thereby initiating cellular stress responses[5]. The HOG pathway is a fungus-specific signaling network that is extensively involved in the regulation of cellular differentiation and virulence factor expression in *Cryptococcus* spp. Previous studies have identified *SSK2* as one of the two significant quantitative trait loci mediating AmB resistance, and its encoded protein is a core component of the HOG pathway, which plays a central role in coordinating cellular responses to environmental stresses such as osmotic pressure[17]. The HOG pathway negatively regulates ergosterol biosynthesis. When this pathway (or its key components, such as Ssk2) is inhibited or absent, negative regulation is lifted, upregulating ergosterol synthesis-related genes (e.g., *ERG11*) and increasing ergosterol content in the cell membrane. The absence of ergosterol content changes observed in the *ssk2Δ*-G4 mutant strain in this study may be attributed to the experimental conditions, which were limited to a single culture medium and thus failed to fully reveal a condition-dependent effect.

The fungicidal mechanism of AmB extends beyond its direct binding to ergosterol in fungal cell membranes to form transmembrane pores, and the oxidative stress it induces also constitutes a key mode of action[18-20]. For example, in *Aspergillus* spp., elevated endogenous ROS levels increase the susceptibility of AmB-resistant strains to antifungal drugs[21]. In *Cryptococcus* spp., AmB induces a robust oxidative burst in the host to kill the fungus and can stimulate host immune responses, exerting synergistic antimicrobial effects.

DCFH-DA fluorescence assays revealed that the point-mutant G4 strain exhibited superior resistance to AmB-induced oxidative stress compared to the *ssk2Δ*-G4+*SSK2*^{WT} strain, maintaining intracellular ROS homeostasis. By integrating transcriptomic data, we found that the catalase gene *CAT1* plays a crucial role in this downstream pathway. Although previous studies indicated that simultaneous deletion of all four catalase genes does not affect *C. neoformans* pathogenicity, related research on *C. gattii* yielded contrasting conclusions: its *cat2Δ* mutant exhibited growth defects under AmB stress, and mice infected with this mutant showed significant differences from controls in survival rate ($P < 0.001$), pulmonary fungal burden ($P < 0.01$), and alveolar structural damage[22].

SSK2^{T265A} *May Serve as a Key Target for the Development of Antimicrobial Drugs for the Adjunctive Treatment of C. gattii Infections*

In addition to carrying a mutation in *SSK2*, the G4

strain also exhibited site-specific variations in *TCO2*. In *C. neoformans,* Tco2 serves as a key sensor kinase in the two-component regulatory system. This system modulates cellular stress responses, drug sensitivity, sexual reproduction, and virulence *via* the Pbs2-Hog1 MAPK signaling pathway. A unique fungal two-component system regulates stress responses, drug sensitivity, sexual development, and virulence in *C. neoformans*[23]. While we attempted to generate a *TCO2* deletion mutant, we were unable to recover viable knockout clones, despite multiple independent transformation events (Supplementary Figure S5). Although this observation is consistent with the essential role of *TCO2*, alternative explanations, including inefficient homologous recombination or positional effects, cannot be excluded. Formal demonstration of essentiality requires conditional knockdown or inducible expression approaches in future studies. Given that *SSK2* exhibited a clear single-point mutation, it was selected for in-depth functional analysis.

After complementing the *SSK2* allele carrying the *SSK2*^{T265A} point mutation into the knockout strain, the AmB resistance phenotype of *ssk2Δ*-G4+*SSK2*^{T265A} was significantly restored. However, this did not reach the G4 level. This discrepancy likely stems from the different promoters used for complementation, leading to a deviation of gene expression levels from the endogenous state.

In summary, antifungal resistance typically arises from the interaction of multiple coexisting mutations, rather than a single genetic variation. This study confirmed that the *SSK2*^{T265A} point mutation is closely associated with the resistance phenotype and functionally contributes to it. The MAPK pathway is crucial for fungal pathogenicity, and its regulation of multiple virulence attributes makes it a potential therapeutic target[24]. Given the high cost and significant toxic side effects of AmB, the development of sensitizers targeting *SSK2*^{T265A} to synergize with AmB against *C. gattii* infection is promising. This approach may reduce drug dosage and toxicity, while maintaining or enhancing therapeutic efficacy.

Limitations of the Study

A major limitation of this study is that the generalizability of our results remains constrained by the small sample size (n = 27) and the restriction of the resistance phenotype to a single clonal background (G4), precluding formal association testing. *SSK2*^{T265A} thus represents a candidate resistance-associated polymorphism that requires further validation in larger cohorts. Two additional limitations should be noted: first, the P_{H3} promoter-driven complementation strategy does not fully recapitulate native-locus regulation; second, the in vivo experiments compared a parental strain with an *SSK2* deletion mutant rather than isogenic strains differing only at Thr265Ala, so the specific contribution of *SSK2*^{T265A} to *in vivo* treatment response awaits further determination.

CONCLUSION

This study suggests that *SSK2*^{T265A} is a key determinant of AmB resistance in *C. gattii*, potentially driving the resistance phenotype through enhanced tolerance to oxidative stress. Furthermore, as no homologous gene for *SSK2* exists in the human genome, *SSK2* may serve as a future research direction in *Cryptococcus* spp. infection. Approaches, such as high-throughput screening of compound libraries or modification of natural small molecules, could be explored to develop specific *SSK2* inhibitors, positioning them as promising candidates for future antifungal drug development.

Funding This work was supported by the National Key Research and Development Program of China (2024YFC2309600), National Natural Science Foundation of China (82370005), Beijing Hospitals Authority “Sailing” Program (ZLRK202513), Beijing Hospitals Authority “Peak” Talent Training Program (DFL20240703), Excellent Talents Program of Capital Medical University (A2310), and the Taishan Scholar Talent Project (No. tsqn202103117).

Competing Interests The authors declare no conflict of interest.

Ethics The use of clinical isolates was approved by the Ethics Committee of Beijing Shijitan Hospital (approval no. sjtky11-1x2022(049)). All animal experiments were approved by the Animal Ethics Committee of Beijing Shijitan Hospital (approval no. sjtky11-1x2022(050)). Eight-week-old female C57BL/6N mice were housed in specific pathogen-free (SPF)-grade barrier facilities at the Experimental Animal Center of China Agricultural University. Environmental conditions were maintained at (22 ± 2) °C, (50 ± 10)% relative humidity, with a 12 h/12 h light/dark cycle. Mice had ad libitum access to autoclaved food and water. Animal health was monitored daily, and mice showing signs of distress (e.g., > 20% weight loss, lethargy, or inability to access food or water) were humanely euthanized.

Authors’ Contributions Conceived of the project

and supervised the research: Xinying Xue and Liye Zhang; Reviewed the manuscript: Chen Wang, Xuelei Zang, and Hengyu Deng; Performed experiments: Hengyu Deng, Xuefeng Zang, Enqi Zhao, Yemei Huang, and Yangyu Zhou; Analyzed and interpreted data: Jing Liu, Wencong He, Chen Yang, Xiaozhuo Dong, Ziqi Zhao, Yuhan Zhou, and Hui Chen; Drafted the manuscript: Hengyu Deng; Edited the manuscript: Hengyu Deng, Xuefeng Zang, and Enqi Zhao; All authors agree to submit the manuscript.

Acknowledgements This work is supported by HPC Platform of ShanghaiTech University.

Data Sharing The raw data of *C. gattii* isolates produced by Illumina sequencing and Oxford Nanopore were deposited in the Sequence Read Archive under the BioProject accession numbers PRJNA721774 and PRJNA721775, respectively, and in the National Microbial Science Data Center, Biological Project number NMDC10019548. The supplementary materials will be available in www.besjournal.com.

Received: March 11, 2026;
Accepted: August 11, 2026

REFERENCES

1. Chang CC, Sorrell TC, Chen SCA. Pulmonary cryptococcosis. Semin Respir Crit Care Med, 2015; 36, 681−91.
2. Wang XC, Mohammad IS, Fan LF, et al. Delivery strategies of amphotericin B for invasive fungal infections. Acta Pharm Sin B, 2021; 11, 2585−604.
3. Ordaya EE, Abu Saleh OM, Vergidis P, et al. Temporal trends in antifungal susceptibility of *Cryptococcus neoformans* isolates from a reference laboratory in the United States, 2011-2021. Mycoses, 2024; 67, e13691.
4. Bagga R, Kavanoor Sridhar K. The silent pandemic: antifungal resistance and the future of invasive fungal disease management. Microorganisms, 2026; 14, 599.
5. Bahn YS, Geunes-Boyer S, Heitman J. Ssk2 mitogen-activated protein kinase kinase kinase governs divergent patterns of the stress-activated Hog1 signaling pathway in *Cryptococcus neoformans*. Eukaryot Cell, 2007; 6, 2278−89.
6. Cingolani P, Patel VM, Coon M, et al. Using *Drosophila melanogaster* as a model for genotoxic chemical mutational studies with a new program, SnpSift. Front Genet, 2012; 3, 35.
7. Liu OW, Chun CD, Chow ED, et al. Systematic genetic analysis of virulence in the human fungal pathogen *Cryptococcus neoformans*. Cell, 2008; 135, 174−88.
8. Chen SCA, Meyer W, Sorrell TC. *Cryptococcus gattii* infections. Clin Microbiol Rev, 2014; 27, 980−1024.
9. Lin JF, Fan YM, Lin XR. Transformation of *Cryptococcus neoformans* by electroporation using a transient CRISPR-Cas9 expression (TRACE) system. Fungal Genet Biol, 2020; 138, 103364.
10. Lozano-Chiu M, Paetznick VL, Ghannoum MA, et al. Detection of resistance to amphotericin B among *Cryptococcus neoformans* clinical isolates: performances of three different media assessed by using E-test and National Committee for Clinical Laboratory Standards M27-A methodologies. J Clin Microbiol, 1998; 36, 2817−22.
11. Fernandes KE, Dwyer C, Campbell LT, et al. Species in the *Cryptococcus gattii* complex differ in capsule and cell size following growth under capsule-inducing conditions. mSphere, 2016; 1, e00350−16.
12. Lee D, Jang EH, Lee M, et al. Unraveling melanin biosynthesis and signaling networks in *Cryptococcus neoformans*. mBio, 2019; 10, e02267−19.
13. Parkhomchuk D, Borodina T, Amstislavskiy V, et al. Transcriptome analysis by strand-specific sequencing of complementary DNA. Nucleic Acids Res, 2009; 37, e123.
14. Espinel-Ingroff A, Chowdhary A, Cuenca-Estrella M, et al. *Cryptococcus neoformans-Cryptococcus gattii* species complex: an international study of wild-type susceptibility endpoint distributions and epidemiological cutoff values for amphotericin B and flucytosine. Antimicrob Agents Chemother, 2012; 56, 3107−13.
15. Córdoba S, Isla MG, Szusz W, et al. Susceptibility profile and epidemiological cut-off values of *Cryptococcus neoformans* species complex from Argentina. Mycoses, 2016; 59, 351−6.
16. Bicanic T, Harrison T, Niepieklo A, et al. Symptomatic relapse of HIV-associated cryptococcal meningitis after initial fluconazole monotherapy: the role of fluconazole resistance and immune reconstitution. Clin Infect Dis, 2006; 43, 1069−73.
17. Roth C, Murray D, Scott A, et al. Pleiotropy and epistasis within and between signaling pathways defines the genetic architecture of fungal virulence. PLoS Genet, 2021; 17, e1009313.
18. Guirao-Abad JP, Sánchez-Fresneda R, Alburquerque B, et al. ROS formation is a differential contributory factor to the fungicidal action of Amphotericin B and Micafungin in *Candida albicans*. Int J Med Microbiol, 2017; 307, 241−8.
19. Sangalli-Leite F, Scorzoni L, Mesa-Arango AC, et al. Amphotericin B mediates killing in *Cryptococcus neoformans* through the induction of a strong oxidative burst. Microbes Infect, 2011; 13, 457−67.
20. Mesa-Arango AC, Scorzoni L, Zaragoza O. It only takes one to do many jobs: amphotericin B as antifungal and immunomodulatory drug. Front Microbiol, 2012; 3, 286.
21. Liang TY, Chen W, Yang XY, et al. The elevated endogenous reactive oxygen species contribute to the sensitivity of the amphotericin B-resistant isolate of *Aspergillus flavus* to triazoles and echinocandins. Front Microbiol, 2021; 12, 680749.
22. Huang YM, Deng HY, Zang XL, et al. The catalase gene *CAT2* and its role in the virulence of one sub-cluster of *Cryptococcus gattii* VGI clinical isolates. Acta Biochim Biophys Sin, 2026; 58, 1866−74.
23. Bahn YS, Kojima K, Cox GM, et al. A unique fungal two-component system regulates stress responses, drug sensitivity, sexual development, and virulence of *Cryptococcus neoformans*. Mol Biol Cell, 2006; 17, 3122−35.
24. La Santrer E, Assunção CB, de Camargo TMN, et al. The protein kinases family in fungi: adaptability, virulence and conservation between species. Front Microbiol, 2025; 16, 1630196.